J Electr Eng Technol.2017; 12(?): 1921-718
http://doi.org/10.???/JEET.2017.12.3.1921

ISSN(Print) 1975-0102
ISSN(Online) 2093-7423

Formulation of the Green's Functions for coplanar Waveguide Microwave Devices as Genetic Algorithm-Based Complex Images

DaJung Han*, ChangHyeong Lee* and Sungtek Kahng†

Abstract – A new Complex Image Method based on Genetic Algorithm (GA) is proposed to calculate the Green's functions of CPW (coplanar waveguide)-type microwave components and antennas. The closed-forms of the spectral-domain integrals are obtained by the GA, avoiding the conventional procedures of the tedious linear algebra and the sampling conditions sensitive to the complex-variable sampling paths adopted in the Prony's and GPOF methods. The proposed method is compared with the numerical Sommerfeld Integral, which results in good agreement.

Keywords: GA; Complex image method; Green's function; MoM: CPW

1. Introduction

Due to the CPW configuration, CPW circuits offer advantages such as the ease of series and shunt connections, low dispersion and low radiation. Much effort has been made in electromagnetically characterizing the CPW structures via the Method of Moment [1-2]. However, the time-consuming nature in the calculation of Green's functions limits the efficient use of the method.

Usually, a CPW structure can be dealt with as a layered media problem where the spectral-domain integral Green's functions are used. When the problem is solved as an MPIE, the complex image method is offered to derive the closed forms of the Sommerfeld-integral type Green's functions and make the entire process of the MoM very efficient. The spectral-domain integrand can be approximated by a sum of complex exponentials by the Prony's and Generalized Pencil of Function (GPOF) methods [3-8]. These conventional methods are sampling-based extrapolation schemes. Like the least square mean method (LSM), the methods [3-8] accompany use of the matrix algebra for eigen-values, and LU or Singular Value Decomposition (SVD). Besides, as the schemes in [3-8] require the samples like the LSM, they get the samples from the sampling paths in the complex-variable plane, and the geometric shape of the path and number of the samples from the chosen path will change and make the procedure tedious, when problems change.

Recently, a number of applications of the GA have been reported for electromagnetics [9-12]. Unlike exhausting stochastic optimization methods, the GA effectively searches the fittest as the solution through selection, crossover and mutation, when the cost function and search space are appropriately written. It is very important to form a pertinent error function for minimization with the help of the GA.

In this paper, a new technique is proposed to calculate the Green's functions of a CPW via the GA-based complex image method. This paper uses the GA to compute the potential Green's functions, while other GA articles cover the change of the geometrical dimensions. This proposed method avoids the conventional procedures of the cumbersome linear algebra (SVD) and the sampling conditions sensitive to the choice of the sampling path. Additionally, using optimization in the GA can provide fewer complex images than those of the conventional methods. The Green's functions are calculated by this method and compared with that of the numerical Sommerfeld integral. The comparison shows high degree of agreement and validity.

2. Green's Functions for a CPW

According to the equivalence theorem, the slot of a CPW structure can be replaced by the synthesis of magnetic dipoles. Fig. 1 shows an x-directed magnetic dipole on the interface between the air and substrate with thickness d. For the substrate, Top is zero and $Bottom$ is $-d$ in the z-axis. The Green's functions of the vector and scalar potentials can be represented as follows.

$$G_{xx}^{F} = G_{xx0}^{F} + G_{xx,sw}^{F} + G_{xx,CI}^{F},$$
$$G_{qm} = G_{qm0} + G_{qm,sw} + G_{qm,CI} \quad (1)$$

G_{xx0}^{F} and G_{qm0} stand for the dynamic images, and $G_{xx,sw}^{F}$ and $G_{qm,sw}$ mean the surface wave terms [3-8]. $G_{xx,CI}^{F}$ and $G_{qm,CI}$ are complex images of vector and scalar potentials, respectively. These terms are directly

† Corresponding Author: Dept. of Information & Telecommunication Engineering, Incheon National University, Korea. (s-kahng@inu.ac.kr)
* Dept. of Information & Telecommunication Engineering, Incheon National University, Korea. ({dajung, Antman}@inu.ac.kr)
Received: January 20, 2016; Accepted: November 4, 2017

obtained without much effort, and are seen as the subtracted ones in equations which follow.

$$G^F_{xx,CI} = \frac{\varepsilon_r \varepsilon_0}{4\pi} \int_{-\infty}^{+\infty} \frac{1}{jk_{0z}} [(R_{TM} - R^0_{TM}) - \sum_{TEpole} \frac{k_{\rho p}}{k_\rho^2 - k_{\rho p}^2} j2k_{1z} \cdot \mathrm{Re}\, s_1] H_0^{(2)}(k_\rho \rho) k_\rho dk_\rho \quad (2)$$

$$G_{qm,CI} = \frac{1}{4\pi\mu_0} \int_{-\infty}^{+\infty} \frac{1}{jk_{0z}} [(R_{TM} + R_{qm}) - \sum_{TE,TMpole} \frac{k_{\rho p}}{k_\rho^2 - k_{\rho p}^2} j2k_{1z} \cdot \mathrm{Re}\, s_2] H_0^{(2)}(k_\rho \rho) k_\rho dk_\rho \quad (3)$$

where

$$R_{TM} = \frac{(k_{1z} - \varepsilon_r k_{0z}) e^{-j2k_{1z}d}}{(k_{1z} + \varepsilon_r k_{0z}) - (k_{1z} - \varepsilon_r k_{0z}) e^{-j2k_{1z}d}} \quad (4)$$

$$R_{qm} = \frac{2k_{1z}^2(\varepsilon_r - 1) e^{-j2k_{1z}d}}{[(k_{1z} + k_{0z}) + (k_{1z} - k_{0z}) e^{-j2k_{1z}d}][(k_{1z} + \varepsilon_r k_{0z}) - (k_{1z} - \varepsilon_r k_{0z}) e^{-j2k_{1z}d}]} \quad (5)$$

$$R^0_{TM} = \sum_{i=0}^{3} (K \cdot e^{-j2k_{1z}d})^{i+1}, \quad K = \frac{1 - \varepsilon_r}{1 + \varepsilon_r} \quad (6)$$

$H_0^{(2)}$ is the second kind of Hankel function of order 0 and j is $\sqrt{-1}$. The bracketed parts of Eq.'s (2) and (3) are denoted as $T^F_{xx,CI}$ and $T_{qm,CI}$. $\mathrm{Re}\, s_1$ and $\mathrm{Re}\, s_2$ mean the residues of R_{TM} and $R_{TM} + R_{qm}$. And, the dispersion relations are

$$k_{0z}^2 = k_0^2 - k_\rho^2, \quad k_0^2 = \omega^2 \varepsilon_0 \mu_0, \quad k_{1z}^2 = k_1^2 - k_\rho^2, \quad k_1^2 = \omega^2 \varepsilon_0 \varepsilon_r \mu_0 \mu_r \quad (7)$$

Without the manipulation like $T^F_{xx,CI}$ and $T_{qm,CI}$, the calculation of Eq. (1) would be time-consuming, because the integrand including only R_{TM} or $R_{TM} + R_{qm}$ is highly oscillatory and slowly decays[1-8].

3. The Conventional Complex Image Method

When the closed forms are to be evaluated by the complex image method[3-8] fast convergent $T^F_{xx,CI}$ and $T_{qm,CI}$ are chosen and can be approximated by the following exponential series.

$$T^F_{xx,CI} = \sum_{m=1}^{M_{CI}} a_m \cdot e^{-b_m k_{1z}}, \quad T_{qm,CI} = \sum_{n=1}^{N_{CI}} u_n \cdot e^{-v_n k_{nz}} \quad (8)$$

where amplitudes a_m and u_n and phases b_m and v_n are complex numbers. Eq. (8) can be carried out by the Prony's or GPOF method including the related sampling scheme and the matrix algebric work for eigen-values, LU-, and SVD procedures which have required conditions [3-8]. The uniform and linear sampling is employed without general rules. Using the Sommerfeld identity, Eq.'s (2) and (3) are converted to the following closed forms of complex images.

$$G^F_{xx,CI} = \sum_{m=1}^{M_{CI}} a_m \cdot \frac{e^{-jk_{0z} r_{b,m}}}{r_{b,m}}, \quad r_{b,m} = \sqrt{\rho^2 + (-jb_m)^2} \quad (9)$$

$$G_{qm,CI} = \sum_{n=1}^{N_{CI}} u_n \cdot \frac{e^{-jk_{0z} r_{v,n}}}{r_{v,n}}, \quad r_{v,n} = \sqrt{\rho^2 + (-jv_n)^2} \quad (10)$$

4. GA-based Complex Image Method

The GA is a global search algorithm. If the objective function adopts the error function of a problem, the GA becomes an error-minimization method. As the progress from generation to generation is made, selection and crossover tend to keep the best chromosome in the population. Mutation enables the search process to escape possible local minima[9-12].

As far as the complex images are to be obtained by error-minimization of the GA, the cases of Eq. (9) and Eq. (10) are separately and parallely carried out. The error functions can be expressed as follows.

$$Err^F_{xx,CI} = | T^F_{xx,CI} - \sum_{m=1}^{\tilde{M}_{CI}} \tilde{a}_m \cdot e^{-\tilde{b}_m k_{1z}} |,$$

$$Err_{qm,CI} = | T_{qm,CI} - \sum_{n=1}^{\tilde{N}_{CI}} \tilde{u}_n \cdot e^{-\tilde{v}_n k_{1z}} | \quad (11)$$

where

$$\tilde{a}_m = \tilde{a}'_m + j \cdot \tilde{a}''_m, \quad \tilde{b}_m = \tilde{b}'_m + j \cdot \tilde{b}''_m \quad (12)$$

$$\tilde{u}_n = \tilde{u}'_n + j \cdot \tilde{u}''_n, \quad \tilde{v}_n = \tilde{v}'_n + j \cdot \tilde{v}''_n \quad (13)$$

For Eq. (9), each of $\tilde{M}_{CI}$ complex images has $\tilde{a}_m$ and $\tilde{b}_m$ which are composed of real variables $\tilde{a}'_m$, $\tilde{a}''_m$, $\tilde{b}'_m$ and $\tilde{b}''_m$ to be used as genes, that is, variables. With the bounds decided, a gene is represented as N_{bit} binary bits, and a chromosome comprizes a set of the genes. A number of chromosomes compose the population and they go through selection, crossover with rate P_{Cr} and mutation with rate P_m per generation. Particularly, during the step of selection, the error function can be evaluated on the same simple sampling path with the conventional methods for convenience. However, the propsed method requires neither the matrix algebra nor the conditions which possibly change in different problems. For Eq. (10), the work is to be done in the same manner.

5. Numerical Results

To present the accuracy of the proposed method, the Green's functions are calculated for the structure in Fig. 1 with $z = z' = 0$, $d = 0.9mm$ and $f_0 = 10GHz$. Regarding the substrate, $\varepsilon_r = 9.8$ and $\mu_r = 1$ are used. Error functions $Err^F_{xx,CI}$ and $Err_{qm,CI}$ are determied to have $\tilde{M}_{CI}$ and $\tilde{N}_{CI}$ chromosomes, respectively as in Eq. (8). $\tilde{a}'_m$, $\tilde{a}''_m$ and $\tilde{b}''_m$ ($\tilde{u}'_n$, $\tilde{u}''_n$ and $\tilde{v}''_n$) range from –5 to 5, but $\tilde{b}'_m$ ($\tilde{v}'_n$) is kep from –5 to zero, which is wide enough for a layered medium. As the number of layers increases, the ranges should be expanded to wider. $\tilde{M}_{CI}$ and $\tilde{N}_{CI}$ set to four, and N_{bit} is five for both the error functions. So, in each of $Err^F_{xx,CI}$ and $Err_{qm,CI}$, sixteen($\tilde{M}_{CI}$ times the number of the genes) GA parameters exist in the population and the population size is set to five times the number of the GA parameters N_{param}. And 40 is given to the number of generations N_{genr}, usually around two times the numer of chrormosomes. The tournament selection and eliticism schemes are decided to govern the GA error-minimization. Additionally, the one-point crossover and the one-point mutation are applied by a rule of thumb. P_{Cr} is determined as 0.6.

First, Fig. 2 shows the behavior of $Err^F_{xx,CI}$ with different values of P_m versus the generation number. The generation number over 20 reveals convergence and no difference between the three curves and is not provided. For $P_m = 0.2$, Err^{TM}_{CI} converges slower than the other cases of $P_m = 0.1$ and $P_m = 0.08$. It is also found that $P_m = 0.08$ is suitable, because a higher mutation rate stirs the direction of solution, and will be used for faster convergence in the solution. The GA conditions are summarized in Table 1.

Next, with all the conditions for the GA application settled down, Fig.'s 3 provide how the sum of the complex images in $Err^F_{xx,CI}$ behaves with the increasing generation number. Through this, we can verify the convergence of the result of the GA and the efficient reduction of the error. Fig.'s 3(a) and (b) show the real and imaginary parts of the sum in Eq. (11), as the generation progresses. The x-axis of Fig.'s 3 is the sample number in the sampling path used for evaluating $Err^F_{xx,CI}$. With the increase of the generation number, the sum converges to $T^F_{xx,CI}$.

Last, G^F_{ii} ($= \frac{4\pi}{\varepsilon_r \varepsilon_0} G^F_{ii}$) and G_Q ($= 4\pi\mu_0 G_{qm}$) are calculated by the proposed method and the numerical Sommerfeld integral, and compared between the two methods to verify the accuracy. With four complex images for both G^F_{ii} and G_Q, it takes this GA-based technique less than half the computation time consumed by the integration on the typical Sommerfeld integral path (SIP).

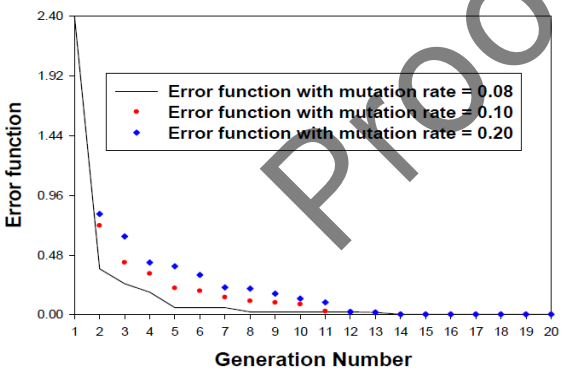

Fig. 2. Error function behavior with mutation rates P_m= 0.08, P_m=0.1 and P_m=0.2 for $z = z' = 0$, d=0.9mm $P_{Cr} = 0.6$ and $f_0 = 10GHz$

Table 1. Conditions for the proposed GA optimization method

Condition	Assianment
1 Gene	5 bits
1 Chromosome	4 Genes
Crossover rate	0.6
1 Population	16 Chromosomes
Mutation rate	0.08
Generation	40

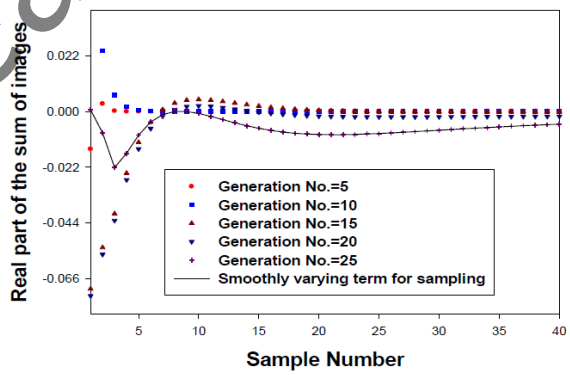

(a)

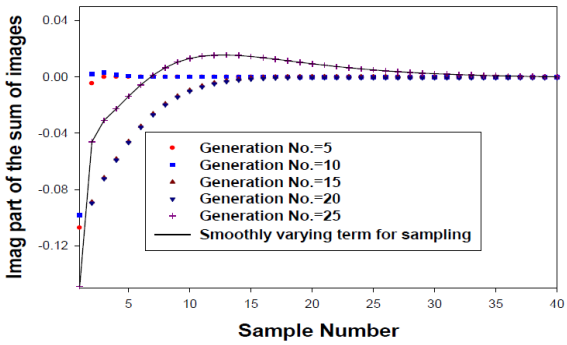

(b)

Fig. 3. Target and the Sum of the Complex Images with generation numbers for P_m=0.08, $z = z' = 0$, d=0.9mm $P_{Cr} = 0.6$ and $f_0 = 10GHz$: (a) Real parts; (b) Imaginary parts

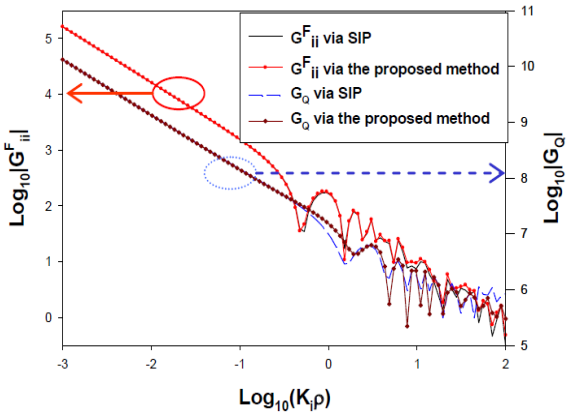

Fig. 4. Comparing the proposed method and the numerical Sommerfeld integral of calculating the Green's functions with $P_m = 0.08$, $z = z' = 0$, $d = 0.9$mm $P_{Cr} = 0.6$ and $f_0 = 10GHz$

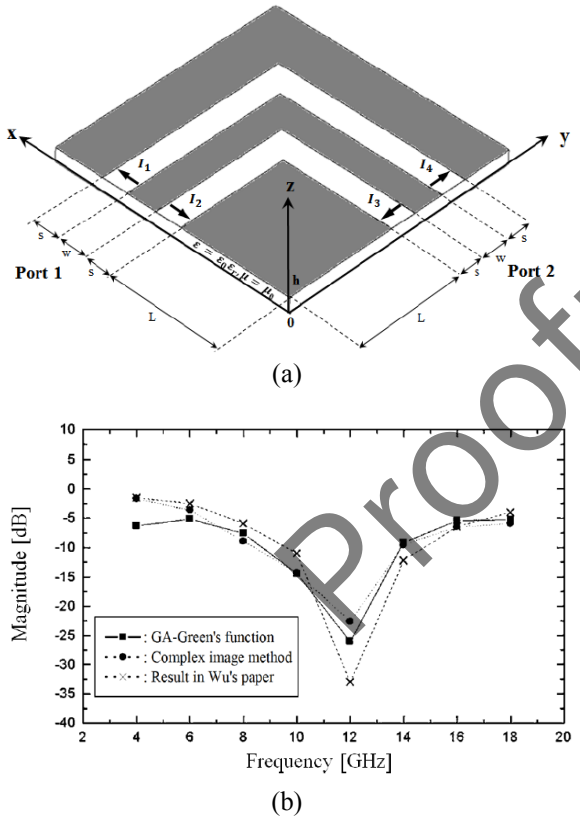

(a)

(b)

Fig. 5. Comparing the proposed method and the other methods in the characterization of a CPW bend: (a) Geometry; (b) Mode-conversion transmission coefficient

Fig. 4 presents excellent agreement between the two methods and validates the accuracy of the proposed method for $z = z'$. Especially, even in the highly oscillatory region, the proposed method calculates the Green's function with little error from the SIP integration advantage. This is applicable to analyze the characteristics of a CPW device. A right-angle CPW bend that is widely used in the PCB artwork is chosen as in [13] as a test example. Fig. 5(a) is the CPW bend excited by an even mode with 0.3 mm, 5 mm, 50 mm, and 0.635 mm as s, w, L, and h, respectively. The mode conversion transmission coefficient from the even-mode to odd-mode is calculated by the proposed method. Its result is plotted in Fig. 5(b) where it is in good agreement with the conventional complex image method and the reference.

6. Conclusion

The problem of CPW type structures is analyzed by a new method employing the GA to obtain complex images. The closed forms of the Green's functions can be calculated with fewer terms by the GA error-minimization. Its accuracy is tested by the comparison with the numerical Sommerfeld integration and they are in excellent agreement.

References

[1] R. Simons et al, "Modeling of Some Coplanar Waveguide Discontinuities," *IEEE Trans. Microwave Theory and Tech.*, vol. MTT-36, pp. 1796-1803, Dec. 1988.

[2] C. Chiu et al, "A Moment-Method Analysis for Coplanar Waveguide Discontinuity Inductances," *IEEE Trans. Microwave Theory and Tech.*, vol. MTT-41, pp. 1511-1514, Sept. 1993.

[3] Y. L. Chow et al, "Closed Spatial Green's Function for the Thick Substrate," *IEEE Trans. Microwave Theory and Tech.*, vol. MTT-39, pp. 588-592, Mar. 1991.

[4] D. G. Fang et al, "Discrete Image Theory for Horizontal Electric Dipoles in a Multilayered Medium," *Proc. IEE*, vol. 135, Pt. Oct. 1991.

[5] R. A. Kipp et al, "Complex Image Method for Sources in Bounded Regions of Multilayer Structures," *IEEE Trans. Microwave Theory and Tech.*, vol. MTT-42, pp. 860-865, May 1994.

[6] M. I. Aksun, "A Robust Approach for the Derivation of Closed-form Green's Functions," *IEEE Trans. MTT*, vol. MTT-44, pp. 651-658, May 1996.

[7] F. Ling et al, " Discrete Complex Image Method for Green's functions of General Multilayered Media," *IEEE Microwave And Guided Wave Letters*, vol. 10, pp. 400-402, Oct. 2000

[8] P. J. Papakanellos et al, "Analysis of an Infinite Current Source Above a Semi-Infinite Lossy Ground Using Fictitious Current Auxiliary Sources in Conjunction with Complex Image Theory Techniques," *IEEE Trans. Antennas and Propagation*, vol. 49, pp. 1491-1503, Oct. 2001.

[9] Y. Rahmat-Samii et al, Electromagnetic Optimization by Genetic Algorithms, New York: John Wiley & Sons, 1999.
[10] S. Kahng, "The Rectangular Power-Bus With Slits GA-Optimized to Damp Resonances," *IEEE Transactions on Antennas and Propagation*, vol. 55, no. 6, pp. 1892-1895, June 2007
[11] G. Byun, J.-C. Hyun, S. M. Seo, and H. Choo, "Optimum Array Configuration to Improve Null Steering Time for Mobile CRPA Systems,", *Journal of Electromagnetic Engineering And Science*, vol. 16, no. 2, pp. 74-79, April, 2016
[12] J. Jeon, S. Kahng, and H. Kim, "GA-Optimized Compact Broadband CRLH Band-Pass Filter Using Stub-Inserted Interdigital Coupled Lines,", *Journal of Electromagnetic Engineering And Science*, vol. 15, no. 1, pp. 31-36, January, 2015
[13] M. D. Wu, S. M. Deng, R. B. Wu, and P. Hsu,"Full-Wave Characterization of the Mode Conversion in a Coplanar Waveguide Right-Angled Bend," *IEEE Trans. Microwave Theory Tech.*, vol. 43, no. 11, pp. 2532-2538, Nov. 1995.

DaJung Han She received B.E degree in electronic engineering from Incheon National University, Incheon, Korea, in 2016. She is currently working toward M. Eng. degree on radio science and engineering at the Department of information and Telecommunication Engineering in the Incheon National University. Her research fields are microwave engineering, RF components and metamaterials.

Changhyeong Lee He received B.E degree in electronic engineering from Incheon National University, Incheon, Korea, in 2016. He is currently working toward M. Eng. degree on radio science and engineering at the Department of information and Telecommunication Engineering in the Incheon National University. His research fields are microwave engineering, RF components and metamaterials.

Sungtek Kahng He received his Ph.D. degree in electronics engineering and communication engineering from Hanyang University, Korea in 2000, with a specialty in radio science and engineering. From 2000 to early 2004, he worked for the Electronics and Telecommunication Research Institute on numerical electromagnetic characterization and developed RF passive components for satellites. In March 2004, he joined the Department of Information and Telecommunication Engineering at the Incheon National University where he has continued research on analysis and advanced design methods of microwave components and antennas, including metamaterial technologies, MIMO communication and wireless power transfer.